

# Structural, Optical, and Photocatalytic Hydrogen Evolution Performance of Undoped and Copper Doped Molybdenum Diselenide Photocatalysts

V. Vanathi, M. Sathishkumar

Department of Electronics, Nehru Arts and Science College, Coimbatore, India

S. Kannan, B. Suresh

Department of Internet of Things, Nehru Arts and Science College, Coimbatore, India

**Abstract** - Copper (Cu) doped molybdenum diselenide ( $\text{MoSe}_2$ ) photocatalysts were successfully synthesized through a hydrothermal method and compared with undoped  $\text{MoSe}_2$ . The formation and purity of the samples were confirmed using XRD, FTIR, and UV-Visible spectroscopy. XRD analysis verified the hexagonal crystal structure, with crystallite sizes of 6.23 nm for pure  $\text{MoSe}_2$  and 12.3 nm for the Cu-doped  $\text{MoSe}_2$  composite. UV-Visible absorption studies revealed band-gap energies of 1.56 eV for the undoped sample and 1.50 eV for the Cu-doped  $\text{MoSe}_2$ , indicating enhanced visible-light absorption due to Cu incorporation. Photocatalytic hydrogen ( $\text{H}_2$ ) evolution experiments under visible-light irradiation showed that pure  $\text{MoSe}_2$  produced  $423 \mu\text{mol g}^{-1} \text{h}^{-1}$  of  $\text{H}_2$ , while the Cu-modified  $\text{MoSe}_2$  achieved a significantly higher activity of  $648 \mu\text{mol g}^{-1} \text{h}^{-1}$  using methanol as a sacrificial agent. Further optimization with 6 mg of Cu- $\text{MoSe}_2$  increased the  $\text{H}_2$  evolution rate to  $894 \mu\text{mol g}^{-1} \text{h}^{-1}$  after 140 minutes. The catalyst maintained a high activity of  $870 \mu\text{mol g}^{-1} \text{h}^{-1}$  even after 10 consecutive cycles, demonstrating the excellent stability and efficiency of the Cu-modified  $\text{MoSe}_2$  for hydrogen evolution applications.

**Keywords:**  $\text{MoSe}_2$ , Copper, hydrothermal method, Hydrogen evolution, Photocatalysts

## 1. INTRODUCTION

Hydrogen ( $\text{H}_2$ ) is widely recognized as a clean, efficient, and sustainable energy carrier capable of addressing the growing global demand for renewable energy. Unlike fossil fuels, hydrogen combustion produces only water as a by-product, making it an environmentally friendly alternative for reducing greenhouse gas emissions [1]. As the world shifts toward greener technologies, developing efficient methods for hydrogen production has become a major research priority. Among the different approaches, photocatalytic water splitting has gained significant attention due to its ability to convert abundant solar energy into chemical fuel [2].

Photocatalysis is an attractive strategy for hydrogen generation because it offers a low-cost, scalable, and environmentally benign route for producing clean energy. The performance of a photocatalyst depends on several key factors, including its ability to absorb visible light, separate charge carriers efficiently, and maintain stability during long-term operation. Therefore, identifying and engineering advanced photocatalytic materials with enhanced optical and electronic properties is crucial to achieving high hydrogen evolution efficiency [3].

Molybdenum diselenide ( $\text{MoSe}_2$ ), a two-dimensional transition metal dichalcogenide (TMD), has emerged as a promising photocatalyst for hydrogen evolution. Its narrow band gap, layered structure, and abundant active edge sites make it highly suitable for visible-light-driven catalytic applications [4]. Additionally,  $\text{MoSe}_2$  exhibits good chemical stability and favorable charge transfer properties, which further support its potential in photocatalytic hydrogen production. However, the photocatalytic activity of pristine  $\text{MoSe}_2$  can still be limited by factors such as recombination of photogenerated electron-hole pairs and insufficient active site exposure [5].

To overcome these limitations, metal doping has been widely explored as an effective strategy to enhance the catalytic performance of  $\text{MoSe}_2$ . Copper (Cu) doping in particular can significantly modify the electronic structure, improve conductivity, and introduce new active sites, thereby facilitating more efficient charge separation and visible-light absorption. Cu incorporation can also increase the crystallite size and create beneficial defects that accelerate hydrogen evolution kinetics. Thus, Cu-doped  $\text{MoSe}_2$  represents a

promising approach for developing high-performance photocatalysts. Motivated by these advantages, the present study focuses on synthesizing and evaluating Cu-doped MoSe<sub>2</sub> for enhanced photocatalytic hydrogen evolution. The main objective is to investigate how Cu incorporation influences the structural, optical, and catalytic properties of MoSe<sub>2</sub> and to compare its performance with undoped MoSe<sub>2</sub>. By optimizing the doping level and reaction conditions, this work aims to develop an efficient, stable, and cost-effective photocatalyst for sustainable hydrogen production under visible-light irradiation.

## 2. MATERIALS AND METHODS

Undoped and Cu-doped MoSe<sub>2</sub> photocatalysts were synthesized using a hydrothermal method. For the preparation of undoped MoSe<sub>2</sub>, stoichiometric amounts of sodium molybdate dihydrate (Na<sub>2</sub>MoO<sub>4</sub>·2H<sub>2</sub>O) and selenourea (CH<sub>4</sub>N<sub>2</sub>Se) were used in a Mo:Se molar ratio of 1:2 to obtain approximately 10 mg of final product. Based on the required amount of MoSe<sub>2</sub>, 9.53 mg of Na<sub>2</sub>MoO<sub>4</sub>·2H<sub>2</sub>O and 9.54 mg of selenourea were accurately weighed and dissolved in 10 mL of deionized water under constant stirring to form a clear precursor solution. For the Cu-doped MoSe<sub>2</sub> sample, the same quantities of Na<sub>2</sub>MoO<sub>4</sub>·2H<sub>2</sub>O and selenourea were dissolved in 10 mL of water, after which 0.5 mol% of Cu relative to Mo was introduced by adding 20  $\mu$ L of a 10 mM Cu(NO<sub>3</sub>)<sub>2</sub>·3H<sub>2</sub>O stock solution, ensuring homogeneous incorporation of Cu into the MoSe<sub>2</sub> matrix. The undoped and Cu-doped precursor solutions were separately transferred into 25 mL Teflon-lined stainless-steel autoclaves, sealed, and heated at 200 °C for 12 hours. After natural cooling to room temperature, the obtained black precipitates were collected by centrifugation and washed several times with deionized water and ethanol to remove residual ions and unreacted species. The purified powders were then dried at 60 °C overnight. To improve crystallinity, the dried samples were optionally annealed at 300–400 °C for 1–2 hours under an inert argon atmosphere. The synthesized catalysts were subsequently used for structural, optical, and photocatalytic hydrogen evolution studies.

The synthesized materials were characterized using various advanced analytical methods. The crystallographic structure was investigated with an X-ray diffractometer (XRD) model X'per PRO. Functional groups were identified through Fourier transform infrared (FTIR) spectroscopy using a Bruker Tensor 37 FTIR spectrometer. UV-Visible analyze were investigated through Double Beam Spectrophotometer UH5300. Photocatalytic hydrogen evolution was performed using a thermal conductivity detector gas chromatograph (Tech, GC-7900) with nitrogen as the carrier gas.

## 3. RESULTS AND DISCUSSION

Figure 1(a) presents the XRD patterns of undoped MoSe<sub>2</sub> and Cu-doped MoSe<sub>2</sub> composites, illustrating their crystallographic features and the structural changes induced by Cu incorporation. The pristine MoSe<sub>2</sub> exhibits well-defined diffraction peaks at 2 $\theta$  values of 13.6°, 31.3°, 37.8°, and 55.8°, which correspond to the (002), (100), (103), and (110) planes of hexagonal MoSe<sub>2</sub>. These reflections are in good agreement with the standard JCPDS card no. 77-1715, confirming the successful formation of a pure hexagonal MoSe<sub>2</sub> phase [6]. In contrast, the Cu-doped MoSe<sub>2</sub> sample shows additional diffraction peaks at 2 $\theta$  values of 41.8° and 46.8°, assigned to the (006) and (200) planes, respectively. The appearance of these new planes indicates that Cu ions are effectively incorporated into the MoSe<sub>2</sub> lattice, causing slight lattice distortion and modifying the crystallographic orientation. This structural alteration also leads to an increase in crystallite size, consistent with the observed XRD peak sharpening and intensity enhancement. Such changes play a vital role in the photocatalytic performance: Cu incorporation can improve the electronic conductivity of MoSe<sub>2</sub>, facilitate faster charge transport, and suppress electron–hole recombination by introducing beneficial defect states. Additionally, the modified lattice structure provides more active edge sites for catalytic reactions. These combined effects contribute to the enhanced hydrogen evolution efficiency observed for the Cu-doped MoSe<sub>2</sub> catalyst compared to the pristine MoSe<sub>2</sub>, demonstrating that controlled Cu doping is an effective strategy to boost the photocatalytic activity of MoSe<sub>2</sub> under visible-light irradiation [7].

Table 1 summarizes the structural parameters of the MoSe<sub>2</sub> and Cu-doped MoSe<sub>2</sub> nanoparticles calculated from the XRD peak at around 31°. Both samples exhibit a similar d-spacing value of 2.848 Å, indicating that the fundamental hexagonal lattice structure of MoSe<sub>2</sub> is retained even after Cu incorporation. However, notable differences arise in the crystallite size, FWHM, dislocation density, and microstrain, reflecting the influence of Cu doping on the structural characteristics. The pristine MoSe<sub>2</sub> shows a crystallite size of 6.23 nm with a relatively broad FWHM of 1.382 radians, which is characteristic of smaller and more strained nanoparticles. In contrast, the Cu-doped MoSe<sub>2</sub> displays a significantly larger crystallite size of 12.3 nm and a narrower FWHM of 0.698 radians, confirming improved crystallinity and reduced peak broadening. The calculated dislocation density and microstrain values also decrease substantially upon Cu incorporation, indicating a reduction in lattice imperfections and internal strain. These

improvements suggest that Cu doping stabilizes the MoSe<sub>2</sub> lattice and promotes more orderly crystal growth. Such structural refinement is beneficial for photocatalytic hydrogen evolution, as larger crystallites with lower defect-induced recombination pathways facilitate more efficient charge separation and faster electron transport [8]. Furthermore, the reduced microstrain and dislocation density help maintain stable active sites during photocatalysis, contributing to the enhanced H<sub>2</sub> evolution performance observed in the Cu-doped MoSe<sub>2</sub> catalyst.

The FTIR spectra presented in Figure 1(b) provide valuable information on the vibrational modes and bonding characteristics of the synthesized MoSe<sub>2</sub> and Cu-doped MoSe<sub>2</sub> photocatalysts. The spectrum of pristine MoSe<sub>2</sub> exhibits distinct vibrational bands in the 400–600 cm<sup>-1</sup> region, corresponding to the characteristic Se–Mo–Se stretching modes, confirming the successful formation of the MoSe<sub>2</sub> lattice and its hexagonal layered structure. Upon Cu doping, noticeable changes appear in the FTIR profile: additional absorption bands emerge in the 600–800 cm<sup>-1</sup> range, which are absent in the undoped sample. These new peaks are attributed to Cu–Se vibrational modes, indicating that Cu atoms are effectively incorporated into the MoSe<sub>2</sub> framework either by substituting Mo sites or occupying interstitial positions. This incorporation leads to slight lattice distortions that strengthen the MoSe<sub>2</sub> structure while reducing intrinsic defects and vacancies [9].

The structural modifications induced by Cu doping play a crucial role in enhancing photocatalytic hydrogen evolution. The formation of Cu–Se bonds and the reduction of defect-induced vibrational disorder contribute to improved crystallinity and more efficient charge transport across the lattice. Additionally, Cu incorporation creates localized electronic states that facilitate better separation of photogenerated electrons and holes, minimizing recombination losses. As a result, the Cu-doped MoSe<sub>2</sub> catalyst possesses more active sites with enhanced stability, enabling superior hydrogen evolution performance compared to pristine MoSe<sub>2</sub> [10]. The FTIR analysis confirms that Cu doping not only modifies the bonding environment but also promotes structural and electronic improvements that directly contribute to the enhanced photocatalytic H<sub>2</sub> evolution.

Figure 2(a) presents the UV–Visible absorption spectra of pristine MoSe<sub>2</sub> and Cu-doped MoSe<sub>2</sub> composites, revealing the impact of Cu incorporation on the optical properties of the material. The undoped MoSe<sub>2</sub> exhibits a strong absorption peak around 795 nm, corresponding to its intrinsic band gap transitions, which reflects the material's ability to harvest visible and near-infrared light. Upon Cu doping, the absorption peak shifts noticeably toward a longer wavelength of approximately 826 nm, indicating a distinct red shift. This shift is attributed to a reduction in the band gap energy, arising from the introduction of Cu-induced defect states and modifications in the electronic structure of MoSe<sub>2</sub> [11]. Such alterations create additional electronic levels near the conduction or valence band, facilitating easier excitation of electrons under visible-light irradiation. The broader and more intense absorption of the CuMoSe<sub>2</sub> composite in the 200–1200 nm range confirms its enhanced light-harvesting capability, particularly in the near-infrared region [12].

The optical band gap of MoSe<sub>2</sub> and CuMoSe<sub>2</sub> was further examined using Tauc plots derived from their UV–Visible absorption spectra, as illustrated in Figure 2(b). The pristine MoSe<sub>2</sub> exhibits a band gap of 1.56 eV, consistent with previously reported values for hexagonal MoSe<sub>2</sub>. Upon Cu incorporation, the band gap decreases slightly to 1.50 eV, confirming a doping-induced modification of the electronic structure. This subtle narrowing of the band gap suggests the formation of intermediate defect states or Cu-related electronic levels within the forbidden energy region [13]. Such defect states lower the energy required for electron excitation, enabling more efficient utilization of visible and near-infrared light. The presence of these additional energy levels is indicative of lattice distortion and electronic rearrangement caused by Cu atoms occupying substitutional or interstitial sites within the MoSe<sub>2</sub> [14]. This reduction in band gap has significant implications for photocatalytic hydrogen evolution. A narrower band gap facilitates enhanced photon absorption and allows the catalyst to generate a higher density of photogenerated charge carriers under the same illumination conditions. Moreover, the introduction of Cu-induced defect states promotes improved charge separation and reduces electron–hole recombination rates by acting as shallow trapping sites that extend carrier lifetimes [15]. As a result, the CuMoSe<sub>2</sub> composite demonstrates superior photocatalytic performance compared to pristine MoSe<sub>2</sub>. The band gap analysis thus reinforces the critical role of Cu doping in tuning the optical and electronic properties of MoSe<sub>2</sub> to achieve enhanced hydrogen evolution efficiency.

Figure 3(a) presents the hydrogen evolution performance of MoSe<sub>2</sub> using 2 mg of catalyst under visible-light irradiation for 240 min in the presence of different sacrificial agents. The results clearly show that the choice of solvent significantly influences the photocatalytic activity, as reflected in the corresponding H<sub>2</sub> generation rates. Pure water showed no detectable hydrogen evolution, indicating that MoSe<sub>2</sub> alone cannot efficiently drive water splitting without a hole-scavenging agent. When triethanolamine and

lactic acid were used, the  $H_2$  evolution increased to 134 and 203  $\mu\text{mol}\cdot\text{g}^{-1}\cdot\text{h}^{-1}$ , respectively, due to their ability to donate electrons and suppress charge recombination. Sodium sulfide further improved the efficiency, delivering 334  $\mu\text{mol}\cdot\text{g}^{-1}\cdot\text{h}^{-1}$ , owing to its strong reducing capability and effective hole-trapping behavior. Among all tested solvents, methanol resulted in the highest hydrogen evolution rate of 423  $\mu\text{mol}\cdot\text{g}^{-1}\cdot\text{h}^{-1}$ , demonstrating its superior role as a sacrificial reagent. Methanol promotes rapid hole consumption and minimizes electron–hole recombination by readily undergoing oxidation, which enables a higher concentration of photogenerated electrons to participate in proton reduction [16]. Additionally, methanol can enhance surface interactions with  $\text{MoSe}_2$ , facilitating improved charge transfer and accelerating reaction kinetics. The remarkable enhancement observed in methanol  $\text{MoSe}_2$  systems confirms that methanol is an effective sacrificial agent for boosting photocatalytic  $H_2$  evolution under visible-light irradiation.

Figure 3(b) illustrates the hydrogen evolution activity of  $\text{CuMoSe}_2$  under visible-light irradiation using 2 mg of catalyst in different sacrificial agents over 240 min. Similar to pristine  $\text{MoSe}_2$ ,  $\text{CuMoSe}_2$  shows no detectable  $H_2$  generation in pure water, confirming that a sacrificial agent is essential to drive the photocatalytic reaction by suppressing electron–hole recombination. When triethanolamine and lactic acid were introduced, the  $H_2$  evolution rates increased significantly to 301 and 469  $\mu\text{mol}\cdot\text{g}^{-1}\cdot\text{h}^{-1}$ , respectively, indicating improved charge separation and enhanced surface redox kinetics. Sodium sulfide further boosted the activity to 511  $\mu\text{mol}\cdot\text{g}^{-1}\cdot\text{h}^{-1}$ , attributable to its strong hole-scavenging capability. Among the tested solvents, methanol exhibited the highest hydrogen evolution rate, reaching 648  $\mu\text{mol}\cdot\text{g}^{-1}\cdot\text{h}^{-1}$ , which highlights its superior ability to promote photocatalytic activity. Methanol acts as an efficient sacrificial agent by readily undergoing oxidation, thereby rapidly consuming photogenerated holes and preventing their recombination with electrons. This leads to a greater availability of electrons for proton reduction, resulting in enhanced hydrogen production [17]. Additionally, methanol can facilitate better surface adsorption and electron transfer pathways, allowing  $\text{CuMoSe}_2$  to utilize visible light more effectively. The pronounced increase in activity compared to other solvents demonstrates that methanol provides the optimal reaction environment for maximizing the  $H_2$  evolution performance of Cu-doped  $\text{MoSe}_2$ .

Figure 4(a) illustrates the influence of catalyst dosage on the hydrogen evolution performance of  $\text{CuMoSe}_2$  in methanol under visible-light irradiation. The catalytic activity increases progressively as the  $\text{CuMoSe}_2$  dosage increases from 2 to 6 mg. At 2 mg of catalyst, the hydrogen evolution rate is 648  $\mu\text{mol}\cdot\text{g}^{-1}\cdot\text{h}^{-1}$  over 240 min, indicating effective utilization of active sites and strong interaction between  $\text{CuMoSe}_2$  and methanol. When the dosage is increased to 4 mg, the  $H_2$  evolution rate improves to 753  $\mu\text{mol}\cdot\text{g}^{-1}\cdot\text{h}^{-1}$ , suggesting that the additional active sites enhance photon absorption and charge separation. The maximum activity is observed at 6 mg, where the rate reaches 894  $\mu\text{mol}\cdot\text{g}^{-1}\cdot\text{h}^{-1}$  within a shorter reaction time of 140 min. This substantial improvement reflects the optimal balance between available catalytic surface area and efficient light harvesting, leading to faster electron transfer and enhanced  $H_2$  generation. Further increasing the dosage to 8 mg and 10 mg does not yield additional improvement, with both dosages showing similar hydrogen evolution values of 894  $\mu\text{mol}\cdot\text{g}^{-1}\cdot\text{h}^{-1}$ . This saturation effect indicates that beyond 6 mg, excess catalyst begins to hinder light penetration due to scattering and shielding effects, limiting the number of photoactive sites that can effectively participate in the reaction [18]. Methanol continues to play a crucial role as an efficient sacrificial agent, rapidly scavenging photogenerated holes and enabling faster electron accumulation on the catalyst surface. This supports sustained hydrogen production even at higher catalyst dosages. The results reveal that 6 mg is the optimal loading for  $\text{CuMoSe}_2$  in methanol, offering maximum photocatalytic efficiency before light-shielding effects restrict further enhancement.

The recycling test for  $\text{CuMoSe}_2$  using 6 mg of catalyst with methanol as the sacrificial agent was conducted over ten consecutive cycles to evaluate the long-term stability and durability of the photocatalyst. As shown in Figure 4(b), the catalyst maintains a remarkably stable hydrogen evolution performance throughout repeated irradiation cycles. In the first cycle,  $\text{CuMoSe}_2$  exhibits an  $H_2$  evolution rate of 894  $\mu\text{mol}\cdot\text{g}^{-1}\cdot\text{h}^{-1}$ , and only a minimal decline is observed as the number of cycles increases. Even after ten runs, the activity remains high at 870  $\mu\text{mol}\cdot\text{g}^{-1}\cdot\text{h}^{-1}$ , corresponding to less than a 3% total reduction. This slight decrease in performance may be attributed to minor surface fouling, marginal structural relaxation, or partial loss of active species during the repeated washing and recovery process [19]. However, the overall retention of activity clearly demonstrates that Cu doping enhances the structural robustness and electronic stability of  $\text{MoSe}_2$ , preventing significant photocorrosion or degradation under prolonged light exposure. The negligible drop in hydrogen evolution efficiency also highlights methanol's effectiveness as a sacrificial agent. Methanol rapidly scavenges photogenerated holes, preventing oxidation-induced damage to the catalyst surface and thereby preserving its active sites over multiple cycles [20]. The consistent performance across all ten cycles confirms that  $\text{CuMoSe}_2$  possesses excellent photochemical stability, strong resistance to deactivation, and reliable recyclability.

## 4. CONCLUSION

In this study, undoped MoSe<sub>2</sub> and Cu-doped MoSe<sub>2</sub> photocatalysts were successfully synthesized using a hydrothermal method, and their structural, optical, and photocatalytic properties were systematically investigated for visible-light-driven hydrogen evolution. XRD and FTIR analyses confirmed the formation of a hexagonal MoSe<sub>2</sub> lattice and verified the effective incorporation of Cu atoms through the appearance of additional diffraction peaks and Cu–Se vibrational modes. Cu doping significantly enhanced the crystallinity, increased crystallite size, and reduced defect density, which collectively contributed to improved charge separation and surface activity. UV–Visible spectroscopy further revealed a noticeable red shift and a decrease in band gap from 1.56 eV (MoSe<sub>2</sub>) to 1.50 eV (CuMoSe<sub>2</sub>), indicating the creation of intermediate energy levels beneficial for visible-light absorption. The photocatalytic H<sub>2</sub> evolution studies clearly demonstrated the superior hydrogen evolution performance of CuMoSe<sub>2</sub>. Methanol proved to be the most effective sacrificial agent for both catalysts, with CuMoSe<sub>2</sub> achieving 648 μmol·g<sup>-1</sup>·h<sup>-1</sup> using only 2 mg of catalyst significantly higher than undoped MoSe<sub>2</sub>. Catalyst dosage optimization revealed that 6 mg of CuMoSe<sub>2</sub> produced the maximum hydrogen evolution rate of 894 μmol·g<sup>-1</sup>·h<sup>-1</sup> within 140 minutes, showing that Cu doping not only enhances activity but also improves light-driven reaction kinetics. The excellent recyclability over ten consecutive cycles, with only a slight decrease from 894 to 870 μmol·g<sup>-1</sup>·h<sup>-1</sup>, confirms the outstanding stability and durability of the Cu-modified catalyst. Overall, the incorporation of Cu into MoSe<sub>2</sub> markedly improves its structural integrity, optical absorption, and charge-transfer behavior, resulting in significantly enhanced hydrogen evolution efficiency. These findings highlight Cu-doped MoSe<sub>2</sub> as a highly promising and stable photocatalyst for sustainable hydrogen production under visible light irradiation.

## REFERENCES

- [1] Nima Mostafazadeh, Reza Dadashi, Masoud Faraji, Morteza Bahram, Electrochemical synthesis of MoSe<sub>2</sub>-Poly (p-Phenylenediamine) nanocomposite on GOS/Graphite substrate for hydrogen production and energy storage applications, *Fuel*, Volume 405, Part B, 2026, 136645, <https://doi.org/10.1016/j.fuel.2025.136645>.
- [2] Can Zhao, Nan Li, Shirui Zhang, Xinding Lv, ALabdulsalam Mohammed Nasser, Yue Li, Shuqian Sun, Jiangquan Ma, Efficient piezo-photocatalytic hydrogen evolution and hydrogen peroxide production: Z-type MoSe<sub>2</sub>/Bi0.5Na0.5TiO<sub>3</sub> bifunctional heterojunction, *Surfaces and Interfaces*, Volume 73, 2025, 107523, <https://doi.org/10.1016/j.surfin.2025.107523>.
- [3] Ramaraj Sukanya, Raj Karthik, Abdullah Al Mahmud, Eithne Dempsey, Deivasigamani Ranjith Kumar, Carmel B. Breslin, Jae-Jin Shim, Synergistic interface of Nb-doped MoSe<sub>2</sub> and NiTe heterostructure enables efficient electrocatalysis for hydrogen evolution, *Electrochemistry Communications*, Volume 180, 2025, 108061, <https://doi.org/10.1016/j.elecom.2025.108061>.
- [4] Yueping Chen, Yuchen Huang, Keying Xiong, Xueyi Ye, Qiqi Liu, Jiarong Zhuang, Yongfan Zhang, Jia Zhu, Cooperative 3d-metals doping MoSe<sub>2</sub> catalysts for enhanced electrocatalytic hydrogen evolution reaction, *Molecular Catalysis*, Volume 566, 2024, 114401, <https://doi.org/10.1016/j.mcat.2024.114401>.
- [5] Siyi Zhang, Ni Hu, Zhenfei Fu, Shilong Suo, Qing Han, Ziwu Han, Ziyue Zhang, Ruiling Zhang, Bing Jin, Zhenhua Zhang, Zhihong Lu, Pengfei Fang, Strain-engineered selenium vacancies in MoSe<sub>2</sub> cocatalysts to redirect photocarrier trapping for efficient hydrogen evolution, *Chemical Engineering Journal*, Volume 525, 2025, 170554, <https://doi.org/10.1016/j.cej.2025.170554>.
- [6] Yang Kuan, Gang Zhao, Tengrui Feng, Luchao Zhao, Qi Wu, The synthesis of Co-doped 1T-rich MoSe<sub>2</sub> effectively enhances electrochemical hydrogen evolution reaction, *International Journal of Hydrogen Energy*, Volume 191, 2025, 152358, <https://doi.org/10.1016/j.ijhydene.2025.152358>.
- [7] Qin Li, Tao Wang, Yun Li, Xingqiang Zhou, Kun Hu, Hui Liu, Quan Qian, Phase synergy and size-dependent regulation in MoSe<sub>2</sub> for enhanced hydrogen evolution reaction, *International Journal of Hydrogen Energy*, Volume 164, 2025, 150828, <https://doi.org/10.1016/j.ijhydene.2025.150828>.
- [8] Gautham Kumar G, P Balaji Bhargav, Nafis Ahmed, Janardhan Reddy Koduru, Strategic integration of Ni<sup>2+</sup> and Cr<sup>3+</sup> bimetallic cations into MoSe<sub>2</sub> for enhanced electrocatalytic hydrogen evolution reaction, *International Journal of Hydrogen Energy*, Volume 175, 2025, 151366, <https://doi.org/10.1016/j.ijhydene.2025.151366>.
- [9] Chang-Yu Hsiao, Phuoc-Anh Le, Ya-Wen Hsu, Jui-Cheng Kao, Chi-Hsuan Chien, Jie Lin, Tzu-Ching Lu, Chun-Wei Pao, Yu-Chieh Lo, Kung-Hwa Wei, Sustainable surface-plasma-exfoliated homogeneous ternary MoSe<sub>2</sub>/WSe<sub>2</sub>/Graphene nanosheets heterostructures as high-efficiency electrocatalysts for hydrogen evolution reaction, *Materials Today Nano*, Volume 32, 2025, 100692, <https://doi.org/10.1016/j.mtnano.2025.100692>.
- [10] Guolin Qian, Yutao Liu, Sili Huang, Songli Dai, Yixin Wang, Xiangyan Luo, Quan Xie, Efficient interfacial charge transfer in the MoSe<sub>2</sub>/SPtSe heterostructure improves the efficiency of hydrogen production from water splitting: A S-scheme photocatalyst, *International Journal of Hydrogen Energy*, Volume 66, 2024, Pages 676-688, <https://doi.org/10.1016/j.ijhydene.2024.04.044>.
- [11] Yaokun Ding, Zhiwei Li, Piaoyun Yang, Yijing Fan, Sha Li, Xianghui Zhang, Yanan Zou, Haoshuang Gu, Zhao Wang, Complementary Nb<sub>2</sub>O<sub>5</sub>/MoSe<sub>2</sub> heterocompositing enables highly selective hydrogen gas sensing at room temperature, *International Journal of Hydrogen Energy*, Volume 106, 2025, Pages 8-15, <https://doi.org/10.1016/j.ijhydene.2025.01.409>.
- [12] Xian-pei Ren, Qi-wei Hu, Fang Ling, Fei Wu, Qiang Li, Liu-qing Pang, Mott-Schottky heterojunction formation between Co and MoSe<sub>2</sub> on carbon nanotubes for superior hydrogen evolution, *New Carbon Materials*, Volume 38, Issue 6, 2023, Pages 1059-1069, [https://doi.org/10.1016/S1872-5805\(23\)60782-6](https://doi.org/10.1016/S1872-5805(23)60782-6).
- [13] Ramaraj Sukanya, Raj Karthik, Abdullah Al Mahmud, Deivasigamani Ranjith Kumar, Eswaran Kamaraj, Carmel B. Breslin, Jae-Jin Shim, Vanadium-doped MoSe<sub>2</sub> Nanosheets: Induced lattice contraction and enhanced conductivity for superior hydrogen evolution reaction, *Electrochemistry Communications*, Volume 175, 2025, 107916, <https://doi.org/10.1016/j.elecom.2025.107916>.
- [14] Lei Liu, Wenkai Zhao, Ting Gao, Enzhou Liu, Haixia Ma, Tao Sun, CoSe<sub>2</sub>/MoSe<sub>2</sub> heterojunction as an efficient electrocatalyst for energy-saving hydrogen production and electro-treatment of organic molecules, *Materials Today Chemistry*, Volume 48, 2025, 103000, <https://doi.org/10.1016/j.mtchem.2025.103000>.
- [15] Daria Baranowska, Jolanta Woronowska, Paweł Sać, Ewa Mijowska, MoSe<sub>2</sub> enriched with borophene towards promotion of electroactivity of Hydrogen Evolution Reaction – in situ and post mortem studies, *Materials & Design*, Volume 256, 2025, 114308, <https://doi.org/10.1016/j.matdes.2025.114308>.

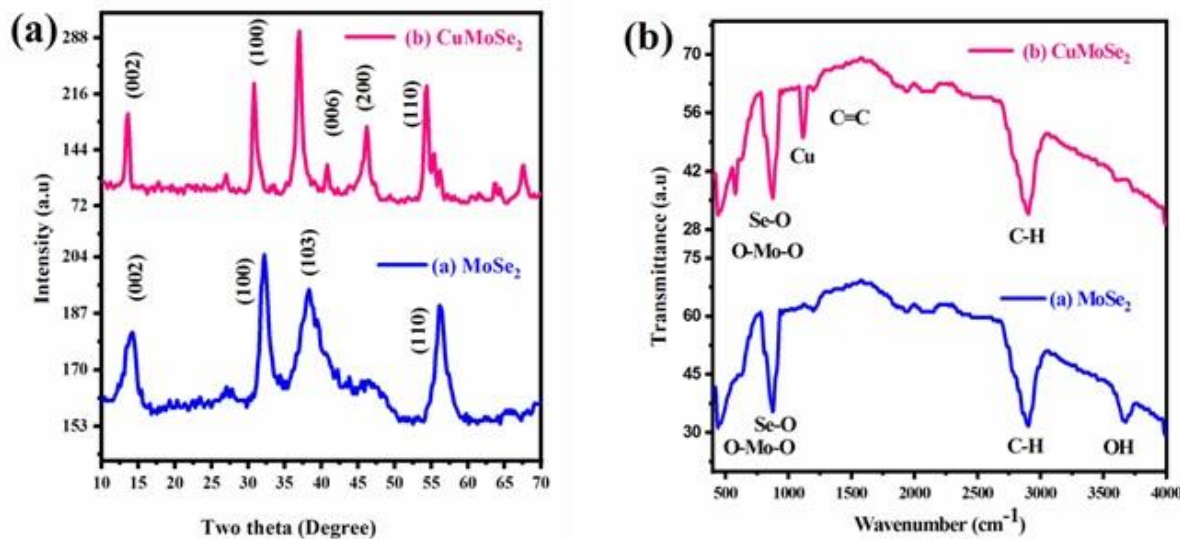
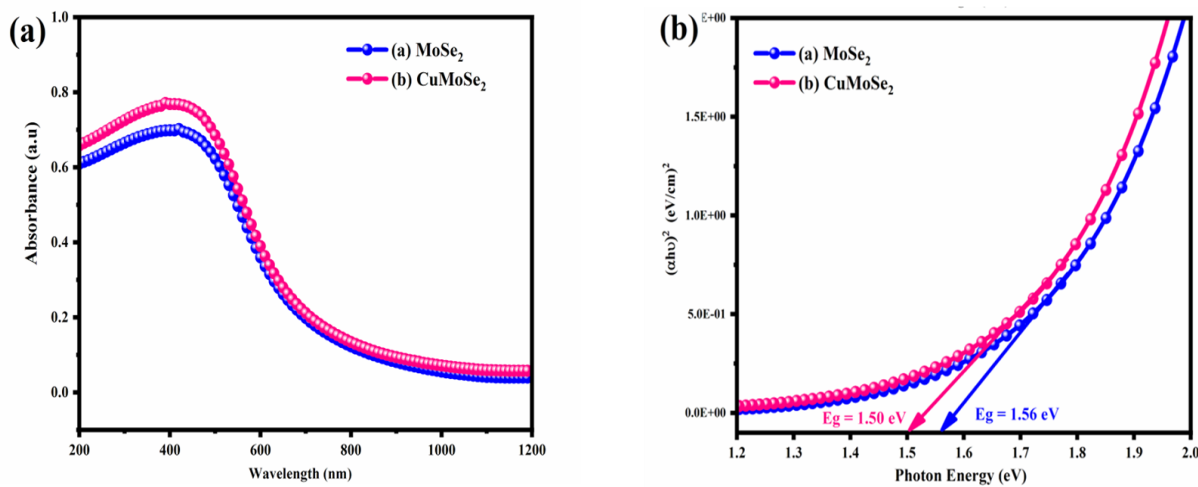
[16] Yuanbo Li, Chunyan Wang, Abdulkader Abdulkayum, Ligang Feng, Advances in green hydrogen generation based on MoSe<sub>2</sub> hybrid catalysts, *Electrochimica Acta*, Volume 503, 2024, 144891, <https://doi.org/10.1016/j.electacta.2024.144891>.

[17] Nitesh Dogra, Paras Agrawal, Sachin Pathak, Rajan Saini, Sandeep Sharma, Hydrothermally synthesized MoSe<sub>2</sub>/ZnO composite with enhanced hydrogen evolution reaction, *International Journal of Hydrogen Energy*, Volume 48, Issue 67, 2023, Pages 26210-26220, <https://doi.org/10.1016/j.ijhydene.2023.03.352>.

[18] Jianjian Yi, Guoxiang Zhang, Xiangyang Cao, Xianglin Zhu, Li Li, Xuyu Wang, Xingwang Zhu, Yanhua Song, Hui Xu, Xiaozhi Wang, Structurally disordered MoSe<sub>2</sub> with rich 1T phase as a universal platform for enhanced photocatalytic hydrogen production, *Journal of Colloid and Interface Science*, Volume 668, 2024, Pages 492-501, <https://doi.org/10.1016/j.jcis.2024.04.166>.

[19] Liping Wang, Junjie Zhao, Xuejuan Tang, Shaofu Kuang, Lizhao Qin, Hua Lin, Qing Li, Green synthesis of MoSe<sub>2</sub> nanosheets based on hydrogen bond with high photodegradation performance, *Surfaces and Interfaces*, Volume 39, 2023, 102956, <https://doi.org/10.1016/j.surfin.2023.102956>.

[20] Vahid Barough, Esmaeil Saievar Iranizad, Amir Bayat, Khadijeh Hemmati, Synthesis of binder-free MoSe<sub>2</sub> nanoflakes as a new electrode for electrocatalytic hydrogen evolution, *Journal of Electroanalytical Chemistry*, Volume 823, 2018, Pages 278-286, <https://doi.org/10.1016/j.jelechem.2018.06.022>.

Figure 1. (a) XRD Pattern (b) FTIR spectra of MoSe<sub>2</sub> and CuMoSe<sub>2</sub> compositesFigure 2. (a) UV-Visible Absorbance Spectra (b) Tauc plots of MoSe<sub>2</sub> and CuMoSe<sub>2</sub> composites

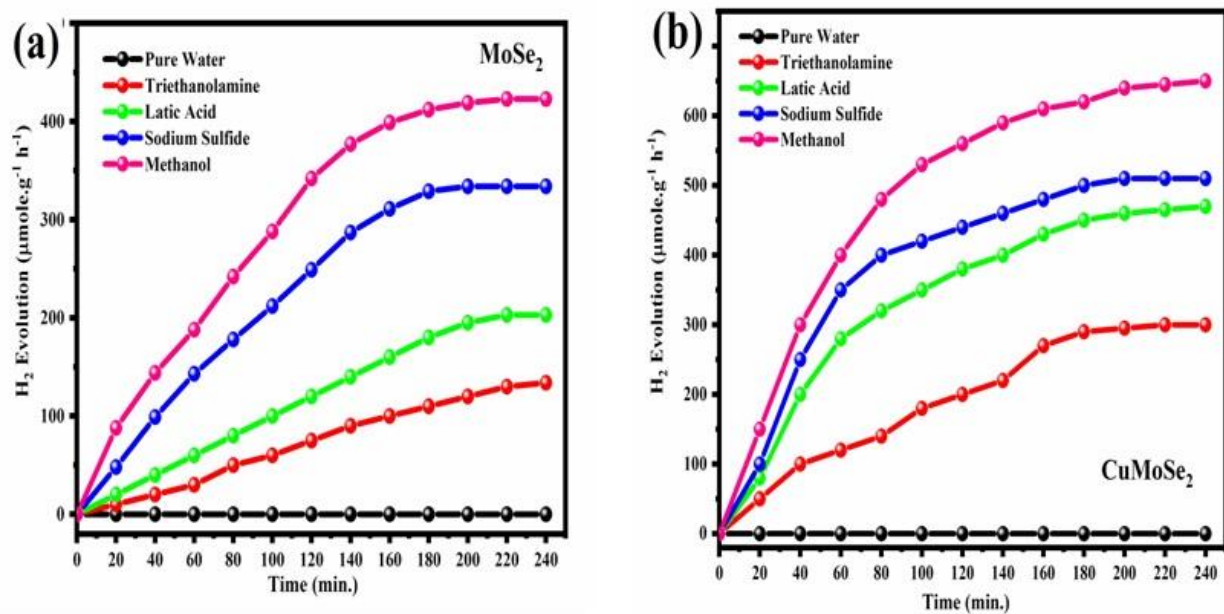
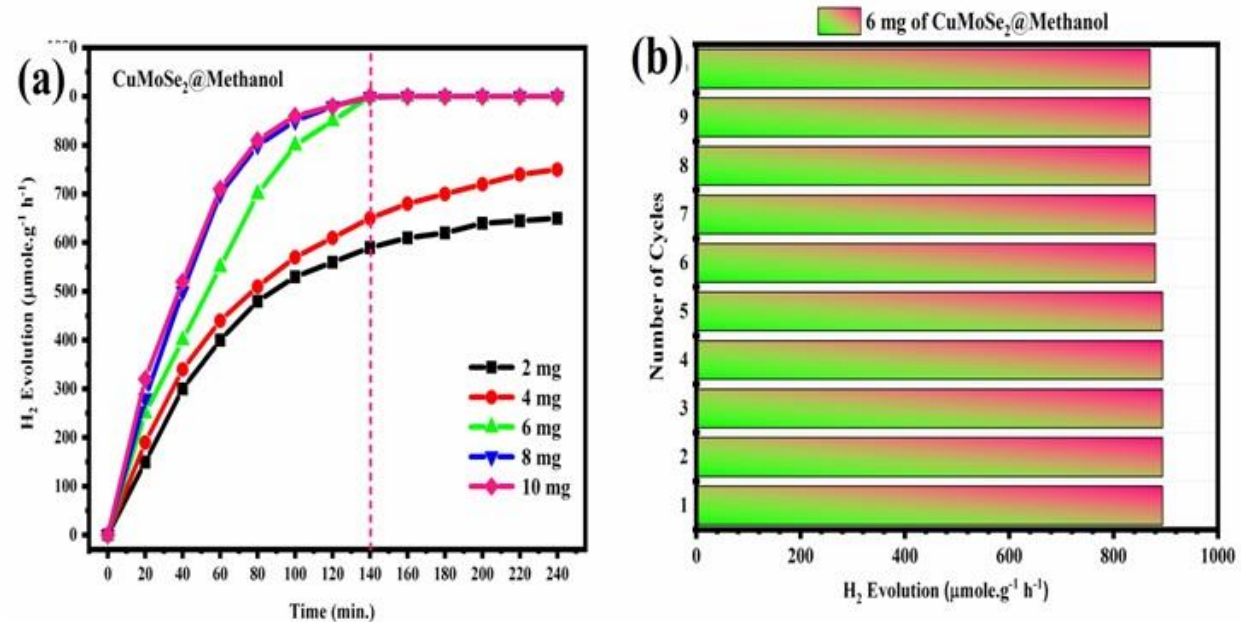
Figure 3.  $\text{H}_2$  evolution of (a)  $\text{MoSe}_2$  (b)  $\text{CuMoSe}_2$  using various sacrificial agentsFigure 4. (a)  $\text{H}_2$  evolution using methanol sacrificial agent at various  $\text{CuMoSe}_2$  dosages(b) Recycling test for 6 mg of  $\text{CuMoSe}_2$  using methanol sacrificial agent

Table 1 Calculated structural parameters of MoSe<sub>2</sub> and CuMoSe<sub>2</sub> composites

Composites	2θ (hkl)	D spacing	FWHM (Radian)	Lattice constants a and c (Å)	crystallite size (nm)	Dislocation Density (δ)	Microstrain (ε)
MoSe <sub>2</sub>	31.3	2.848	1.382	2.848	6.23	0.004644	0.005496
CuMoSe <sub>2</sub>	31.1	2.848	0.698	2.848	12.3	0.001193	0.002794